

Constraining Supersymmetry using the relic density and the Higgs boson

Sophie Henrot-Versillé¹, Rémi Lafaye², Tilman Plehn³, Michael Rauch⁴, Dirk Zerwas¹, Stéphane Plaszczyński¹, Benjamin Rouillé d'Orfeuil¹, Marta Spinelli¹

¹*LAL, CNRS/IN2P3, Orsay Cedex, France*

²*LAPP, Université de Savoie, IN2P3/CNRS, Annecy, France*

³*Institut für Theoretische Physik, Universität Heidelberg, Germany and*

⁴*Institute for Theoretical Physics, Karlsruhe Institute of Technology (KIT), Karlsruhe, Germany*

Recent measurements by Planck, LHC experiments, and Xenon100 have significant impact on supersymmetric models and their parameters. We first illustrate the constraints in the mSUGRA plane and then perform a detailed analysis of the general MSSM with 13 free parameters. Using SFitter, Bayesian and Profile Likelihood approaches are applied and their results compared. The allowed structures in the parameter spaces are largely defined by different mechanisms of dark matter annihilation in combination with the light Higgs mass prediction. In mSUGRA the pseudoscalar Higgs funnel and stau co-annihilation processes are still avoiding experimental pressure. In the MSSM stau co-annihilation, the light Higgs funnel, a mixed bino–higgsino region including the heavy Higgs funnel, and a large higgsino region predict the correct relic density. Volume effects and changes in the model parameters impact the extracted mSUGRA and MSSM parameter regions in the Bayesian analysis.

Contents

I. Introduction	2
II. Supersymmetric parameters	3
III. Annihilation channels	4
IV. Data and analysis setup	5
V. mSUGRA analysis	6
A. Profile likelihood for positive μ	6
B. Bayesian probability for positive μ	9
C. Negative μ	10
VI. MSSM analysis	10
VII. Outlook	13
References	15

I. INTRODUCTION

When trying to understand the physics of the electroweak scale we encounter a set of experimental and theoretical problems. First, the discovery of a narrow, most likely fundamental Higgs scalar means that the hierarchy problem is now real [1]. Second, dark matter search experiments like Xenon100 are starting to cut into the available parameter space of a weakly interacting dark matter particle [2]. Third, in the 7 TeV and 8 TeV runs there seems to be no hint for any physics beyond the Standard Model at ATLAS, CMS, and LHCb.

On the other hand, the particle nature of dark matter is the most attractive hypothesis. The key observable in such models is the current dark matter density in the Universe. The Planck collaboration has recently released their data on the cosmological microwave background temperature anisotropies [3]. In the Λ CDM scenario they determine the dark matter density $\Omega_{\text{cdm}} h^2$ with an unprecedented accuracy [4].

If we take for example the approximate gauge coupling unification [5] as a motivation to look for a weakly interacting ultraviolet completion of the Standard Model we are still driven to supersymmetry [6]. The discovery of a Higgs boson in the Minimal Supersymmetric Standard Model (MSSM) mass range [7] gives no reason to modify or abandon this hypothesis. Moreover, alternative structures like extra dimensions or little-Higgs-like models find themselves under at least as much experimental pressure as supersymmetry. The question we should answer at the end of the first phase of LHC is which part of the MSSM parameter space is consistent with all available (non)-observations.

Even in supersymmetric models the nature of dark matter remains an open question. While in the MSSM the only available TeV-scale dark matter candidate is the lightest neutralino [8], very weakly interacting dark matter particles might exist at much lower masses [9]. In the light of many indirect constraints on neutralino-induced higher-dimensional operators we can extend the dark matter fermion to a Dirac spinor [10], predicting interesting but still unobserved sgluon signatures at the LHC [11]. Recent years have seen a large effort to condense properties of different dark matter models into effective theory concepts [12]. In spite of all these options we will limit ourselves to the case where the entire observed dark matter density is due to a single state, the lightest Majorana neutralino. If this hypothesis comes under experimental pressure, this might serve as a motivation for more elaborate dark sectors, but we will see that there is no such pressure.

Our analysis is based on the SFITTER toolkit which determines the underlying parameters of complex models in the absence of simple one-to-one correlations of observables and parameters. We explore the parameter space with Monte Carlo Markov Chains of the likelihood function. This tool also permits to compare the results within the same framework, using either Bayesian or Profile Likelihoods analysis. It has previously been applied to the problem of the determination of supersymmetric parameters [13], including a bottom-up renormalization group analysis and experimental information on production rates [14], as well as Higgs coupling measurements [15]. In this paper we will study the impact of the recent LHC Higgs measurements and of the $\Omega_{\text{cdm}} h^2$ measurement by Planck. We will compare the latter to the WMAP-9year results [16].

We will use mSUGRA [17] as an illustration of the constraints than can be put through the use of this full set of measurements. This step is necessary to study what happens in models where the a-priori relatively unrelated weak dark matter sector, Higgs sector, and strongly interacting sector of the MSSM are strongly linked by a high-scale construction. The main emphasis of our study is the challenging study of a TeV-scale MSSM. The determination of its parameters is the ultimate goal in order to infer from data whether the parameters are unified at a higher scale. This determination should shed light on which scenarios of SUSY breaking might be favored [14]. Therefore we use a 13 parameter MSSM, which is a technically challenging endeavor because of the large number of parameters. In addition we use the top mass as an input and as a parameter. This additional parameter helps fine tuning the Higgs mass for dark matter annihilation.

Similar studies have been performed by other groups considering different models: for instance, FITTINO has studied the impact of LHC data and WMAP-7year results [18] on two models, mSUGRA and a non-universal Higgs model, the MASTERCODE group has performed a likelihood study of the same mSUGRA and non-universal Higgs models including Xenon100 results [19]. A specific analysis with Planck data, the Higgs mass measurement, and Xenon100 in the TeV-scale MSSM exists but which focuses on light neutralino dark matter [20]. Results similar to ours have recently been published in Ref. [21] for mSUGRA and by the BayesFITS group, including the study of a 9-parameter MSSM in Ref [22]. Compared to this model, we are letting the data constrain more parameters, rendering the determination more complex. A non-exhaustive list of other, similar analyses is given in Ref. [23].

II. SUPERSYMMETRIC PARAMETERS

With the limited number of actual measurements entering this analysis it is clear that we will not be able to make any definite statements about a full TeV-scale supersymmetric mass spectrum. We will illustrate our results using two model setups. As a first test we will study the unified gravity-mediated mSUGRA model, this will give us some ideas about how strongly unified models can accommodate the various data constraints. Second, in a proper bottom-up approach we will consider a free TeV-scale spectrum, reduced to the subset of relevant mass parameters.

The strongly constrained mSUGRA model is described by three mass parameters defined at the unification scale: m_0 , the common scalar breaking mass parameter, $m_{1/2}$ the common gaugino breaking mass parameter and A_0 , the common trilinear mass parameter. In addition, $\tan \beta$ as the ratio of the vacuum expectation values of the two Higgs doublets encodes successfully electroweak symmetry breaking. Finally, we have to fix the sign of the higgsino mass parameter μ . In our conventions the term $-\mu$ appears in the lower-right off-diagonal terms of the neutralino mass matrix. The off-diagonal entry in the stop mass matrix is $m_t(A_t - \mu \cot \beta)$ [24]. Because the parameter A_t is the key parameter in the computation of the light Higgs mass around 126 GeV we quote the approximate solution to the renormalization group evolution [25],

$$A_t = A_0 \left(1 - \frac{0.75}{\sin^2 \beta}\right) - 3.5m_{1/2} \left(1 - \frac{0.41}{\sin^2 \beta}\right) \approx \begin{cases} 0.62A_0 - 2.8m_{1/2} & \text{for } \tan \beta = 1 \\ 0.25A_0 - 2.1m_{1/2} & \text{for } \tan \beta \gg 1. \end{cases} \quad (1)$$

The larger $\tan \beta$ becomes the more the weak-scale parameter A_t is driven by $m_{1/2}$. For $m_{1/2} > 0$ we essentially almost find $A_t < 0$.

When we use renormalization group equations to run high-scale supersymmetry breaking parameters to the weak scale, fixed to 1 TeV as suggested by Ref. [26], we need to ensure that we successfully generate the observed electroweak symmetry breaking. It is convenient to include $\tan \beta$ as a mSUGRA model parameter, but this choice mixes high-scale mass parameters with a TeV-scale ratio of vacuum expectation values. To be more consistent in the definition of the mSUGRA parameter space we can avoid $\tan \beta$ and replace it with the appropriate mass parameters evaluated at the unification scale [25],

$$\begin{aligned} \mu^2 &= \frac{m_{H_u}^2 \sin^2 \beta - m_{H_d}^2 \cos^2 \beta}{\cos(2\beta)} - \frac{1}{2}m_Z^2 \\ 2B\mu &= (m_{H_d}^2 - m_{H_u}^2) \tan(2\beta) + m_Z^2 \sin(2\beta). \end{aligned} \quad (2)$$

H_u has a tree-level coupling to up-type fermions, while H_d couples to down-type fermions. The parameter $B\mu$ accompanies the doublet mixing $H_u^0 H_d^0$. Instead of m_{H_j} and $\tan \beta$ we can use B and μ and the correct value of m_Z as mSUGRA model parameters. For the profile likelihood approach the two parametrizations are equivalent. However, for the Bayesian approach they will lead to different priors and hence to different results [13]. In terms of $\tan \beta$ a flat prior in the high-scale mass parameters corresponds to the prior [27]

$$\left| \frac{m_Z}{2\mu^2} (m_{H_u}^2 + m_{H_d}^2 + 2\mu^2) \frac{1 - \tan^2 \beta}{(1 + \tan^2 \beta)^2} \right|, \quad (3)$$

defined at the electroweak scale. At large values of $\tan \beta$, the Jacobian in Eq.(3) scales like $1/\tan^2 \beta$, which means that the high-scale flat prior prefers small values of $\tan \beta$. When we define the entire MSSM parameter set at the TeV-scale, Jacobians like the one shown in Eq.(3) are simply an effect of our freedom to choose our MSSM model parameters.

In computing the weak-scale mass spectrum in the simple mSUGRA model we start with the independent GUT-scale parameters, evolve the soft SUSY-breaking parameters to the TeV scale, and compute the corresponding masses of the supersymmetric states. SFITTER primarily relies on SUSPECT2 [24] for the renormalization group evolution and the computation of the supersymmetric mass spectrum. In addition, we use SoftSUSY [28] to test our results. Because of the different behavior of the squark and the gaugino masses in the m_0 vs $m_{1/2}$ plane [29] some complexity of the mSUGRA model arises through parameter correlations.

The most general MSSM contains a large number of parameters, of which we identify 17 which will affect current LHC and dark matter measurements [13]. Moreover, the absence of evidence for supersymmetric particles at the LHC leads us to effectively decouple some of the masses to values well about the TeV scale.

In this analysis all squark mass parameters with the exception of the stop sector are fixed at 2 TeV. The same value is assumed for the gluino mass parameter M_3 . This way gluinos and light-flavor squarks move outside the region excluded by the LHC. The question of the bias introduced by this assumption will be addressed later. The trilinear mass parameter A_b is assumed to be zero. The first-generation slepton parameters are identified with their second-generation counter parts. This leaves 13 supersymmetric parameters to be explored: $\tan\beta$, the electroweak gaugino mass parameters (M_1, M_2), the smuon and stau sectors ($M_{\tilde{\mu}_{L,R}}, M_{\tilde{\tau}_{L,R}}, A_\tau$), the stop sector ($M_{\tilde{q}_{3L}}, M_{\tilde{t}_R}, A_t$), the heavy Higgs mass m_A , and the higgsino mass parameter μ .

Effectively, this reduced parameter space decouples the strongly interacting MSSM sector from the weak sector with the relevant dark matter and Higgs predictions. The only remaining strongly interacting particle in the picture is the top squark with its large impact on the Higgs sector — related to its particular relevance in the solution of the hierarchy problem. Since the uncertainties in the top quark mass are non-negligible, and because the induced parametric uncertainties for example for the light MSSM Higgs mass cannot be neglected, we include it as an additional model parameter in the mSUGRA as well as in the MSSM analysis.

The prediction of the light MSSM Higgs mass is calculated with SUSPECT2 [24] while the Higgs branching ratios are computed using SUSY-HIT and HDECAY [30]. The supersymmetric contribution to the cold dark matter density is calculated with MICROMEAS [31]. For the electroweak precision observables we rely on SUSYPOPE [32]. Finally, we use SUSPECT2 [24] and MICROMEAS [31] to compute the B observables and $(g-2)_\mu$.

III. ANNIHILATION CHANNELS

To study the effect of the measured dark matter relic density on the supersymmetric parameter space we need to take into account the fact that data drive us into a few distinct parameter regimes [21]. These structures combined with the light Higgs mass prediction will lead to well-defined regions of the mSUGRA and MSSM parameter spaces which are consistent with all current data.

The first is the light Higgs funnel region where the mass of the lightest Higgs boson is about twice the mass of the LSP. The leading contribution to dark matter annihilation is then the s -channel annihilation via the lightest Higgs, dominantly decaying to b quarks. As a consequence of the tiny width of the lightest Higgs, $\Gamma_h \sim 5$ MeV, the LSP mass has to be finely adjusted to produce the correct range in $\Omega_{\text{cdm}} h^2$. A small, $\mathcal{O}(10\%)$ higgsino component of the LSP will give the correct relic density. Technically, this precise tuning will be a challenge for our parameter analysis.

The same s -channel annihilation can proceed via the heavy Higgs bosons A, H , where the widths can be very large and the level of tuning will be smaller. Unlike the h -funnel, this A -funnel region can extend to arbitrarily large LSP masses, provided the Higgs masses follow the LSP mass. The main heavy Higgs decay channels are $b\bar{b}$ and $t\bar{t}$, because, in these kinds of two-Higgs-doublet models, the massive gauge bosons decouple from the heavy Higgs sector.

A second annihilation topology gives rise to the τ co-annihilation region [33]. Here, the mass difference between for example the stau as the next-to-lightest supersymmetric particle and the LSP needs to be small, of the order of few per-cent or less. If the LSP has a large higgsino component the annihilation then proceeds via an s -channel tau lepton into a tau and a pseudo-scalar Higgs. On the scale of the size of LHC detectors the stau could in such scenarios become stable. However, the higgsino component is not required for co-annihilation to work. If instead the selectron or smuon are the next-to-lightest supersymmetric particles and essentially mass degenerate with the LSP they could lead to the same effect. In the squark sector the same mechanism exists for the lightest top squark [34] or other squark next-to-lightest superpartners. However, given the preference of the Higgs mass measurement for heavy stop masses we find it outside our preferred parameter range.

In the absence of a significant mass splitting between the lightest neutralino and lightest chargino, co-annihilation in the neutralino-chargino sector can accelerate dark matter annihilation in the early universe [35]. Because the necessary mass degeneracy cannot appear for a light bino, the LSP will be dominantly wino or higgsino. Two final states occur for neutralino-chargino co-annihilation: if the t -channel neutralino or chargino exchange dominates, massive gauge bosons and eventually light-flavor quarks will be produced in the

measurement	value and error
m_h	$(126 \pm 0.4 \pm 0.4 \pm 3) \text{ GeV}$ [39]
$\Omega_{\text{cdm}} h^2$ Planck	$0.1187 \pm 0.0017 \pm 0.012$ [4]
$\Omega_{\text{cdm}} h^2$ WMAP-9year	$0.1157 \pm 0.0023 \pm 0.012$ [16]
$\text{BR}(B_s \rightarrow \mu^+ \mu^-)$	$(3.2_{-1.2}^{+1.5} \pm 0.2) \times 10^{-9}$ [40]
$\text{BR}(b \rightarrow X_s \gamma)$	$(3.55 \pm 0.24 \pm 0.09) \times 10^{-4}$ [42]
Δa_μ	$(287 \pm 63 \pm 49 \pm 20) \times 10^{-11}$ [43]
m_t	$(173.5 \pm 0.6 \pm 0.8) \text{ GeV}$ [44]

TABLE I: Some of the key measurements used in our analysis, including the error. The last number is the theoretical uncertainty on the supersymmetric prediction, except for the $\text{BR}(b \rightarrow X_s \gamma)$ and m_t for which no theoretical uncertainty is considered.

annihilation process. If, in contrast, a heavy Higgs in the s -channel dominates, the final state will dominantly consist of third-generation quarks.

Finally, the focus point region [25, 36] is characterized by large m_0 , small $m_{1/2}$, and accidentally small $|\mu|$. Close to this region of parameter space where μ changes sign, we find a higgsino-like light neutralino which couples to gauge bosons and can annihilate into the WW channel. For mSUGRA, this area is highly reduced by both Xenon100 [19] and LHC gluino search limits [37, 38].

IV. DATA AND ANALYSIS SETUP

In Table I we list the main experimental inputs to our analysis. The Higgs mass measurement at the LHC considered in this study is from ATLAS [39]. Because it comes with a sizeable theoretical error from the supersymmetric prediction an improved measurement, such as the measurement of $\text{BR}(B_s \rightarrow \mu^+ \mu^-)$ by CMS [41], will not affect our results. The different production and decay channels of the Higgs boson [45] provide some additional information on its couplings [15], but with little impact on the supersymmetric parameter space when added to the Higgs mass and the flavor observables [46]. We consider the updated result $\text{BR}(B_s \rightarrow \mu^+ \mu^-) = (2.9_{-1.0}^{+1.1} \pm 0.2) \times 10^{-9}$ [47] in the mSUGRA section. It has no impact on the results so we stick to the value quoted in Table I for the MSSM study.

A major point of this study is on the new measurement of the cold dark matter density of the universe by the Planck collaboration. We compare it with the WMAP-9year measurement. In both cases we use the values from the more precise measurements in the Λ CDM scenario:

- Planck: $\Omega_{\text{cdm}} h^2 = 0.1187 \pm 0.0017$ [4]
This is a combination of Planck data, large scale polarization WMAP data [48], ACT/SPT [49], and baryon acoustic oscillation measurements (BAO) [50].
- WMAP-9year: $\Omega_{\text{cdm}} h^2 = 0.1157 \pm 0.0023$ [16]
This combines WMAP data, BAO and a Hubble parameter measurement [51].

Some tension remains between Planck's estimated H_0 value and the direct measurements used in the WMAP-9year analysis. We compare the two approaches to see whether the difference in central values and errors leads to differences in the constraints on the supersymmetric parameter space.

An additional dark matter related input is the upper limit on the elastic LSP–Nucleon cross section as function of the LSP mass from the analysis of the Xenon100 225 days \times 34 kg dataset [2].

For $\tan \beta > 50$ the branching ratio of the flavor violating decay $B_s \rightarrow \mu^+ \mu^-$ is particularly sensitive to supersymmetric contributions [52] and hence constraining. The measurement of $\text{BR}(b \rightarrow X_s \gamma)$ tends to disfavor $\mu < 0$ for large $\tan \beta$ [53]. The difference in the predicted and measured anomalous magnetic moment of the muon tends to accommodate large $\tan \beta$ and to disfavor $\mu < 0$ [54]. The reason for this definite sign preference in μ is a possible cancellation in the off-diagonal entries of the third generation scalar mass matrices. The top mass [44] is both, a model parameter and a measurement.

In SFITTER the statistical errors on the measurements are treated as Gaussian or Poisson where appropriate. The systematic errors are correlated if originating from the same source. Theoretical uncertainties are treated with the RFIT scheme [13, 15, 55], *i.e.* using flat errors in a profile likelihood construction.

The analysis proceeds in two steps. First, we construct a fully exclusive log-likelihood map in the model parameters using a set of Markov Chains with a Breit-Wigner proposal function. Each chain has a different starting point. Their convergence is checked by comparing the mean values and variances of each chain through the quantity \hat{R} [56] as implemented in Ref. [57]. The maximum over the set of Markov Chains $\max[\hat{R}]$ will approach unity if the chains have converged and cover the full parameter space.

On this exclusive log-likelihood map we then define two types of projections: a profile likelihood based on the Frequentist approach and a marginalization as an example of the Bayesian approach. The absolute scales of the projected log-likelihood values in the two approaches can not be used to compare them.

In 2-dimensional standard contour plots we identify the interesting parameter regions and their correlations. In these regions we explore the structures locally, using a modified version of MINUIT [58] to refine the location of the minima.

V. MSUGRA ANALYSIS

The strongly constrained mSUGRA parameter space is governed by a very small number of parameters. They are linked to the TeV-scale masses via coupled renormalization group running and therefore highly correlated. Knowing the light Higgs mass further constrains the parameter space through the stop sector. In such cases the standard Markov Chain Monte Carlo methods give the most stable results, so we do not use the weighted Markov Chains which are otherwise optimized for a small number of parameters [13, 59]. For each sign of μ we travel in the 5-dimensional parameter space of m_0 , $m_{1/2}$, A_0 , $\tan\beta$, and m_t with 49 Markov chains of 200000 points each, giving us 9.8 million accepted samplings. Our parameter space is bounded by $m_0 < 5$ TeV, $m_{1/2} < 5$ TeV, $|A_0| < 4$ TeV, and $\tan\beta < 61$. The convergence criterion finds $\max[\hat{R}] \approx 1.008$, indicating a good convergence of the chains.

A. Profile likelihood for positive μ

Because a priori the sign choice $\mu > 0$ is favored by the Δa_μ measurement, we will discuss it first. The four different 2-dimensional profile likelihoods for $\mu > 0$ are shown in Figure 1. All of them use the recent Planck measurement of the cold dark matter density. The first observation is the absence of a clear preference in the m_0 values. In contrast, the dark matter relic density favors three distinct regions in $m_{1/2}$, as introduced in Section III:

1. the narrow stau co-annihilation strip with $m_{1/2} < 1$ TeV and $m_0 < 500$ GeV at moderate $\tan\beta$. The mass of the lightest slepton $\tilde{\tau}_1$ is very close to the LSP mass.
2. the A -funnel region with $m_{1/2} \approx 1.7$ TeV and $\tan\beta \approx 50$, where the LSP mass around 745 GeV is roughly half the heavy Higgs mass $m_{A,H}$ and the heavy Higgs states have a sizeable width to allow for a spread-out s -channel annihilation.
3. the h -funnel region with $m_{1/2} \approx 130$ GeV, where the bino-LSP mass of 60 GeV is about half the mass of the lightest Higgs. The dominant dark matter annihilation process is the resonant s -channel annihilation via the lightest Higgs boson. Because of the link between the LSP and gluino masses, this channel could typically be ruled out by direct LHC searches.

Two additional well-known parameter regions [21] are explicitly excluded by our bounds of the parameter space. We nevertheless confirm that they would appear in an extended parameter scan, namely

4. the focus point region [25, 36] with its WW annihilation channel at $m_0 \in [3, 20]$ TeV, and $m_{1/2} \in [0.2, 20]$ TeV. This region is mainly excluded by Xenon100 [19], except for a few points such as SPS2 [60] which is ruled out by LHC exclusions [37, 38].
5. the stop co-annihilation strip with $A_0/m_0 \in [3, 6]$ and $A_0/m_0 \in [-15, -3]$.

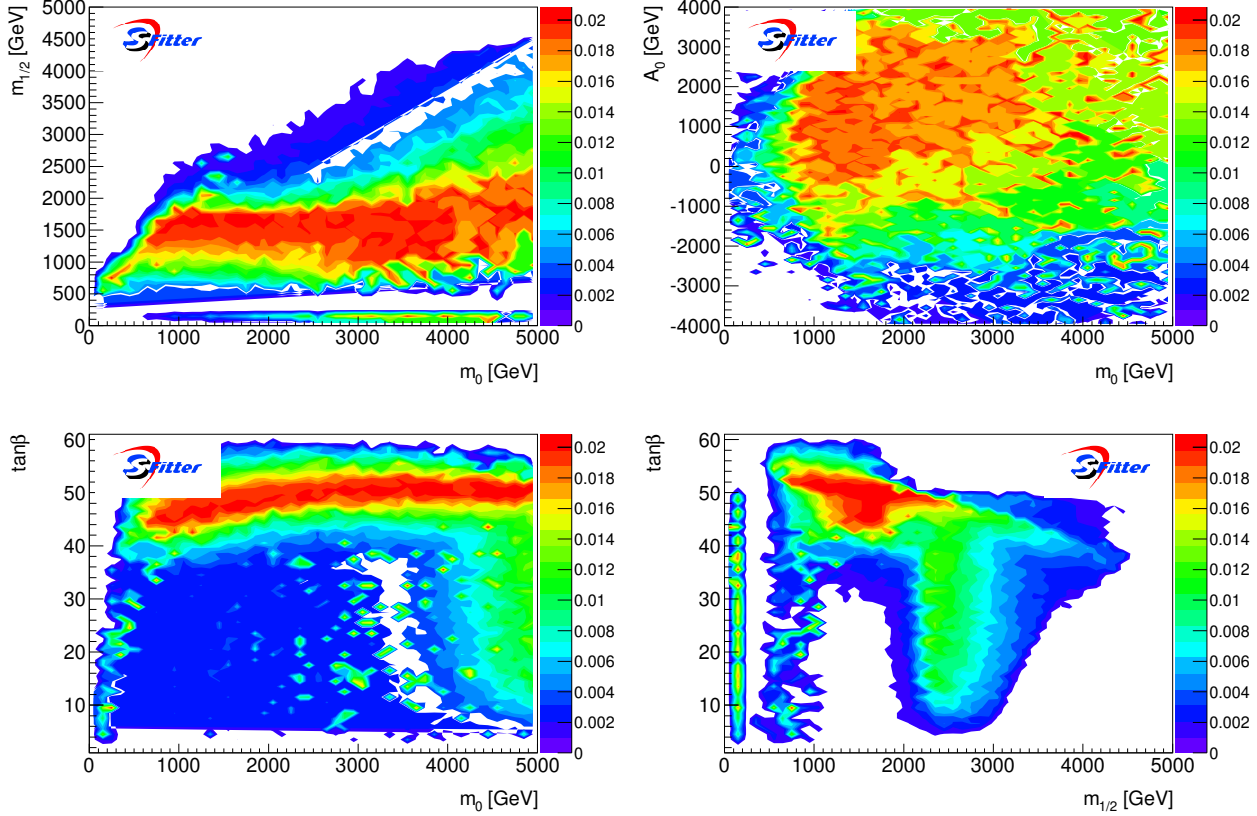


FIG. 1: Profile likelihood projections onto the $(m_0, m_{1/2})$ plane, the (m_0, A_0) plane, the $(m_0, \tan \beta)$ plane, and the $(m_{1/2}, \tan \beta)$ plane. All results are based on the Planck measurement and assume $\mu > 0$.

In particular the size of the A -funnel region is then defined by the light Higgs mass constraint. Relating the Higgs mass constraint we need to be a little careful. In Section II we have seen that the relevant trilinear coupling A_t mostly scales with $m_{1/2}$. The main contribution to the light Higgs mass comes from the two top squarks, so the relatively heavy Higgs mass pushes the preferred physical stop masses to large values. According to Eq.(1) negative values of A_0 will increase $|A_t|$, leading to a larger stop mass splitting and hence a smaller mass of the lighter stop mass eigenstate. Indeed, we find that the different measurements prefer $A_0 > 0$, while large negative A_0 values and low m_0 values are disfavored by the Higgs mass constraint.

In the lower panels of Figure 1 we see that large $\tan \beta$ values are clearly favored, independently of m_0 . An exception appears only for large m_0 values, where the allowed range in $\tan \beta$ becomes sizeable. The dark blue area for $500 \lesssim m_0 \lesssim 3000$ GeV and $\tan \beta < 35$ is disfavored by the Higgs mass measurement. Large values of $\tan \beta$ are needed to increase its value, while the stop masses are fairly independent of m_0 . Dark matter plays the key role in excluding the white area around $m_0 \approx 3.5$ TeV.

	m_0	$m_{1/2}$	$\tan \beta$	A_0	m_t	$-2 \log L/\text{dof}$	$-2 \log L/\text{dof (LHCb)}$
co-annihilation	442	999	24.6	-1347	174.0	49.0/75	49.0/75
A -funnel	1500	1700	46.5	2231	173.9	48.9/75	49.2/75
h -funnel	4232	135	26.6	-2925	174.2	46.1/75	46.1/75

TABLE II: Illustration of best-fit parameters for the three regions of mSUGRA: A -funnel, h -funnel, and co-annihilation with $\mu > 0$. The corresponding $-2 \log L$ is given in column 7. The last column illustrates the impact on the new LHCb measurement of $\text{BR}(B_s \rightarrow \mu^+ \mu^-)$.

	co-ann	A	h		co-ann	A	h		co-ann	A	h		co-ann	A	h
\tilde{e}_L	792	1860	4210	\tilde{g}	2178	3596	476	\tilde{q}_L	2020	3527	4174	h	123.0	123.0	124.8
\tilde{e}_R	575	1621	4223	$\tilde{\chi}_1^0$	429	745	59	\tilde{q}_R	1939	3397	4192	H	1423	1498	3624
$\tilde{\nu}_{eL}$	788	1858	4209	$\tilde{\chi}_2^0$	809	1379	118	\tilde{b}_1	1754	3046	3190	A	1423	1498	3624
$\tilde{\mu}_L$	792	1860	4210	$\tilde{\chi}_3^0$	-1407	-1588	-507	\tilde{b}_2	1849	3101	3877	H^+	1425	1500	3625
$\tilde{\mu}_R$	575	1621	4223	$\tilde{\chi}_4^0$	1412	1603	512	\tilde{t}_1	1426	2771	2374				
$\tilde{\nu}_{\mu L}$	788	1858	4209	$\tilde{\chi}_1^+$	810	1379	119	\tilde{t}_2	1791	3105	3212				
$\tilde{\tau}_1^-$	430	1103	3920	$\tilde{\chi}_2^+$	1412	1603	514								
$\tilde{\tau}_2^-$	756	1666	4062												
$\tilde{\nu}_{\tau L}$	744	1661	4061												

TABLE III: Supersymmetric particles' masses (in GeV) for the three best-fit points shown in Table II. They correspond to the favored regions: A -funnel, h -funnel, and co-annihilation with $\mu > 0$.

A similar feature, albeit a small anti-correlation, can be seen in the $m_{1/2}$ vs $\tan\beta$ plane. The slight anti-correlation for large $\tan\beta$ and $m_{1/2}$ is attributed to the Higgs masses. First, the light Higgs mass increases with a larger stop mass and hence growing $m_{1/2}$, so smaller values of $\tan\beta$ become possible. Moreover, the dark matter relic density can be reached through the pseudoscalar annihilation funnel. Because a decrease of $\tan\beta$ increases the heavy Higgs masses, the dark matter relic density forces a simultaneous increase in $m_{1/2}$ and hence the LSP mass. This keeps the mass ratio around 2:1.

In Table II we show the best-fit solutions in the mSUGRA parameter space. In the last column we compare the log-likelihood obtained with the updated measurement of $\text{BR}(B_s \rightarrow \mu^+ \mu^-)$ showing that the results do not depend on this observable. The three preferred regions with their distinct dark matter annihilation processes are kept separate. For the A and h funnels in mSUGRA the LSP has roughly the same gaugino-higgsino composition. It is dominantly a bino and annihilates to $b\bar{b}$ final states. In the co-annihilation point the annihilation goes into $\tau\tau$ final states, helped by the process $\tilde{\tau}\tilde{\chi}_1^0 \rightarrow A\tau$. The general preference for large m_0 values from the dark matter constraints and the lightest Higgs mass overrides the favorite regions for $(g-2)_\mu$, which until recently dominated the corresponding analyses. The Δa_μ contribution to $-2\log L$ becomes a constant offset.

The influence of the top mass and its uncertainty cannot be neglected, as we see for example in the h -funnel region. Compared to the nominal value of 173.5 GeV in Table I the best fit result shown in Table II is increased by 0.7 GeV. This increase leads to a slight reduction of M_1 by at most 0.1 GeV and an increase of μ from 350 GeV to 490 GeV. For the LSP this implies a larger mass by about 0.8 GeV and a decreased higgsino component by almost 50%. In parallel, the Higgs mass increases by 0.2 GeV, as compared to the prediction using the nominal top mass. Combining the two mass shifts and the decreased LSP coupling to the Higgs leads to the correct value of $\Omega_{\text{cdm}} h^2$.

The complete mass spectrum of the sparticles corresponding to the three points is given in Table III. The h -funnel has a relatively light gluino of 476 GeV, driven by the low LSP mass. The squark masses turn out heavy. Because the available mSUGRA limits from ATLAS [37] and CMS [38] are calculated for different values of $A_0 = 0$ and $\tan\beta = 10$ the results cannot be applied directly, but it is clear that this parameter point will be excluded by inclusive squark and gluino searches at the LHC. The only obvious way to hide light gluinos in these analyses would be to complement them with mass-generate squarks, such that the decay jets become too soft to be observed [61]. However, in mSUGRA the squark masses are linked to the stop masses, and light stop masses are ruled out by the Higgs mass constraint. Hence, for mSUGRA the list of non-excluded dark matter annihilation channels given in Section III is reduced to stau co-annihilation and the A -funnel within the parameter space considered in this analysis.

As mentioned above, one of the key motivations of this analysis is to see the impact of the recent Planck measurements, in comparison to the WMAP-9year results. The most visible difference can be observed in the $(m_{1/2}, A_0)$ plane in Figure 2. The general features are very similar. In addition, the separation between the light Higgs funnel region and the rest of the plane becomes clearer with the new and improved Planck measurement. This reflects the essentially equivalent central values but smaller error bars on $\Omega_{\text{cdm}} h^2$.

B. Bayesian probability for positive μ

To this point we have only relied on profile likelihood projections. While Frequentist and Bayesian approaches cannot be expected to give equivalent answers (because they ask different questions) they can still give complementary information. In Figure 3 we show the Bayesian projections onto the $(m_0, m_{1/2})$ and $(m_0, \tan \beta)$

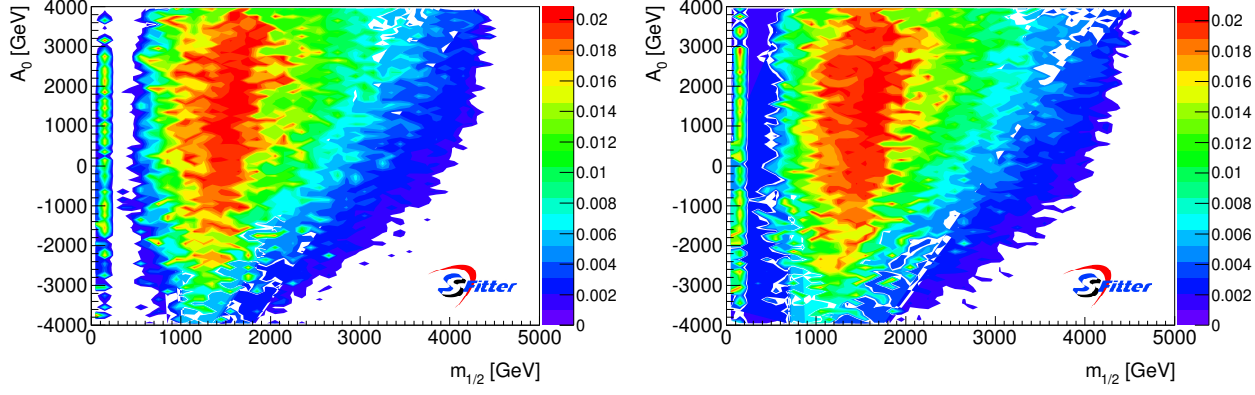


FIG. 2: Profile likelihood projection onto the $(m_{1/2}, A_0)$ plane using the Planck (left) and WMAP (right) measurements.

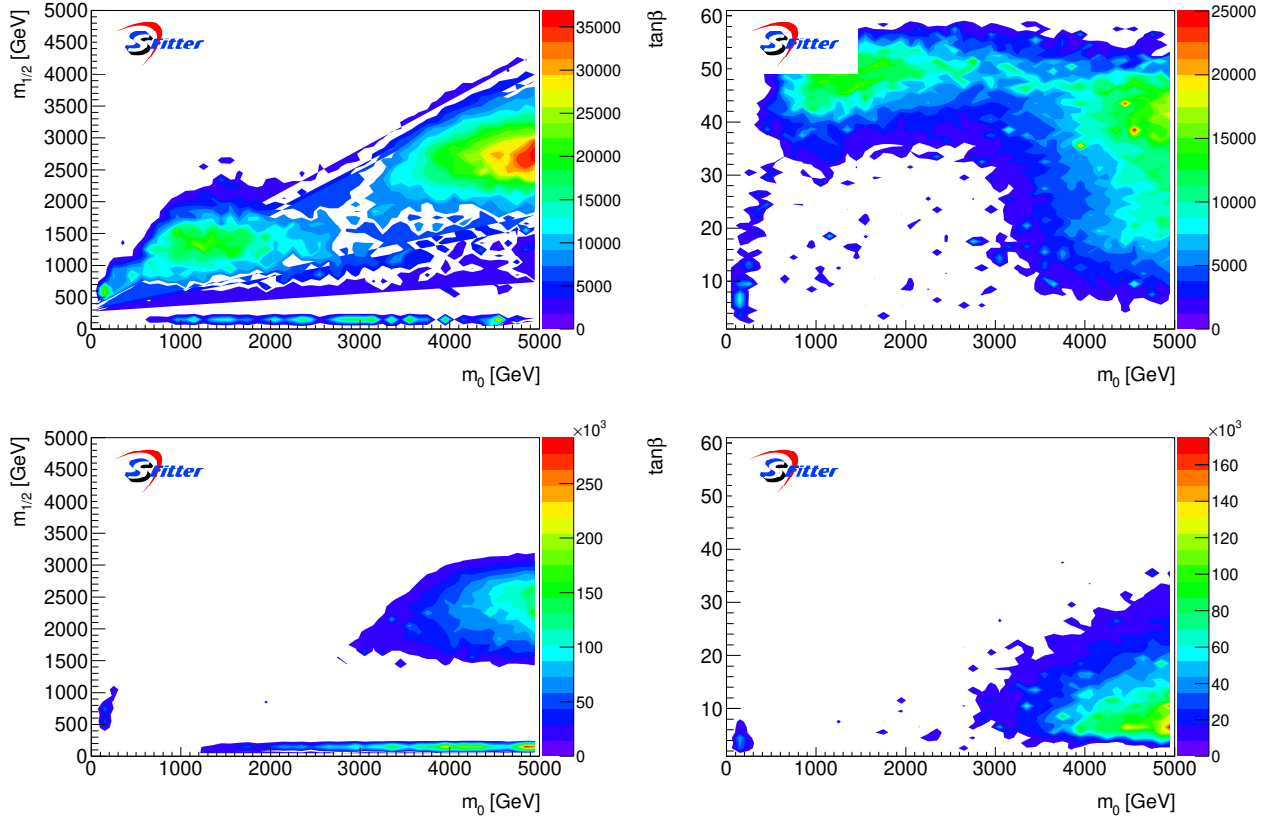


FIG. 3: Bayesian projection onto the $(m_0, m_{1/2})$ plane (left) and the $(m_0, \tan \beta)$ plane (right) for a $\tan \beta$ -flat prior (top) and a high-scale flat prior (bottom). All results are based on the Planck measurement and assume $\mu > 0$.

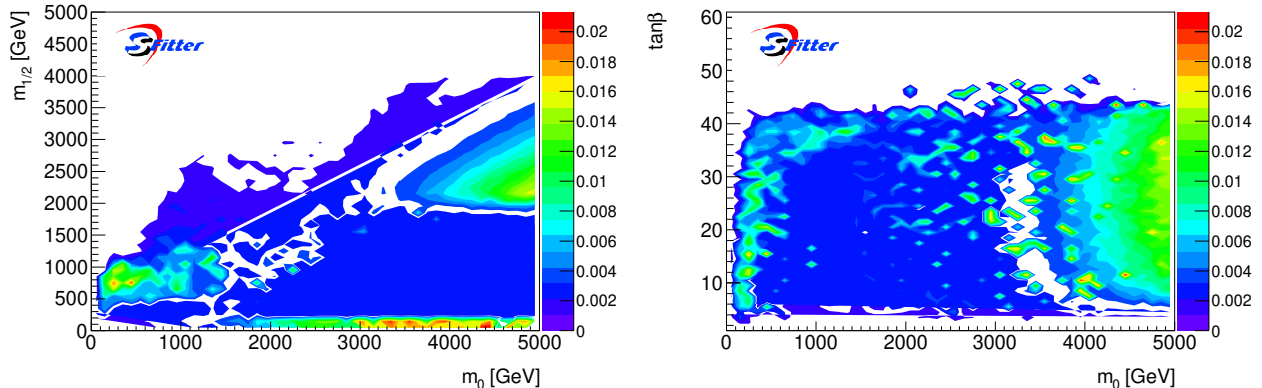


FIG. 4: Profile likelihood projections onto the $(m_0, m_{1/2})$ and $(m_0, \tan\beta)$ planes. All results are based on the Planck measurement and assume $\mu < 0$.

planes, using the consistent $\tan\beta$ -flat and high-scale flat priors discussed in Section II.

Both, the $(m_0, m_{1/2})$ plane and the $(m_0, \tan\beta)$ plane using the consistent high-scale flat prior show similar features as for the profile likelihood approach. First, there is the well separated low- $m_{1/2}$ solution from the light Higgs funnel. Second, the narrow co-annihilation strip is hard to see, but still present. Finally, the A -funnel bulk region is divided in low and high m_0 values and shows a clear preference for $m_0 > 4.5$ TeV and $m_{1/2} \approx 2.8$ TeV. This can be explained by the volume effect when integrating over $\tan\beta$, A_0 , and m_t : the best-fit value around $m_{1/2} = 1.5$ TeV has a low probability for most $\tan\beta$ values, except for $\tan\beta = 40 - 50$. In contrast, for $m_{1/2} \approx 2.5$ TeV the preferred region extends over almost all $\tan\beta$ values. In general, m_t moves significantly below its nominal value to accommodate the A -funnel region, but covering a larger range for large m_0 . All of these features can also be seen in the profile likelihood analysis, but they only develop two well defined preferred regions after we integrate the Bayesian probabilities.

The whole picture changes significantly when we instead use a low-energy prior, flat in $\tan\beta$, in the Bayesian analysis. In the $(m_0, m_{1/2})$ plane the low- m_0 part of the bulk solution vanishes. In the $(m_0, \tan\beta)$ plane, suddenly low $\tan\beta$ values are favored. This is simply an effect of the relative difference in priors shown in Eq.(3). Such a prior dependence suggests that our information is not yet sufficient to draw conclusions on Bayesian favored regions.

C. Negative μ

Finally, we turn to $\mu < 0$. From the argument above we would expect similarly good fits with a finite log-likelihood offset from Δa_μ . In Figure 4 we indeed observe similar features as for $\mu > 0$, but on the absolute scale of the log-likelihood only the h -funnel region at low $m_{1/2}$ retains its features. The A -funnel region at $m_{1/2} \approx 1.5$ TeV is now clearly disfavored.

The correlation in $\tan\beta$ vs m_0 sheds some light on this feature: for large values of $\tan\beta$ and $\mu < 0$ values the cancellation in the off-diagonal entries of the third generation squark mass matrices fails. This will lead to light sbottoms and stops with very large couplings to the heavy Higgs states. They will trigger conflicts with heavy flavor measurements and eventually with the perturbativity of the renormalization group equations. The best solutions for $\mu < 0$ are hence restricted to the light Higgs funnel and the co-annihilation regions at low values of $m_{1/2}$.

VI. MSSM ANALYSIS

Going from a strongly constrained model such as mSUGRA to the MSSM increases the number of free parameters. The ultimate goal of such an analysis is to shed light, with enough experimental constraints, on which scenarios of SUSY breaking are favored. We choose to constrain 13 parameters plus the top mass.

Our parameter space is bounded by $\tan\beta < 61$, $(M_1, M_2) < 4$ TeV, $(M_{\tilde{\mu}_{L/R}}, M_{\tilde{\tau}_{L/R}}, M_{\tilde{q}_{3L}}, M_{\tilde{t}_R}) < 5$ TeV, $(|A_\tau|, |A_t|) < 4$ TeV, $m_A < 5$ TeV and $|\mu| < 2$ TeV. This number is considerably larger than the number of strong constraints or measurements we apply in our analysis, rendering the analysis quite complex in terms of likelihood maximization. On the other hand, now, different sub-sectors of parameters largely decouple. We analyze the MSSM parameter space with 100 Markov chains of 200000 points each, leading to a total number of 2×10^7 of tested samples. For the convergence parameter $\max[\hat{R}]$ typical values are 1.005 and better.

The measured light Higgs mass essentially depends on three parameters: the heavy Higgs mass scale m_A , which has to be large to accommodate the 126 GeV measurement; $\tan\beta$ which has to be large enough to not delay the decoupling regime in m_A ; and finally the geometric mean of the two stop masses $\sqrt{m_{\tilde{t}_1} m_{\tilde{t}_2}}$, which again has to be large. In terms of MSSM parameters the latter needs to be computed from the three entries in the stop mass matrix, including A_t . The stop masses are the key parameters, but are neither strongly related to the dark matter sector nor to the light-flavor squark-gluino mass plane. In addition, they are directly linked to the solution of the hierarchy problem and hence to the motivation of supersymmetry.

The light-flavor squark masses and the gluino mass are experimentally constrained by searches for jet plus missing energy in LHC experiments. While it is entirely possible to avoid these limits in certain decay setups, the strongly interacting supersymmetric masses are likely to lie in the several-TeV range. This tendency towards a heavy strongly interacting SUSY sector is in line with the stop mass constraint from the Higgs sector.

The dark matter sector is most strongly constrained by our requirement that the entire relic density is due to the LSP, in our case the lightest neutralino. The neutralino masses and couplings depend on the four parameters M_1 , M_2 , $\tan\beta$ and μ . The link between the dark matter sector and other sectors rests on the different LSP annihilation channels, as explained in detail in the mSUGRA section. For a sufficiently fast LSP annihilation we cannot rely on generic scattering processes, for example with a t -channel slepton, squark, or chargino. Instead, the easiest ways to reach the observed $\Omega_{\text{cdm}} h^2$ values are light and heavy Higgs funnels and co-annihilation.

In general, the range of μ is strongly limited as the light charginos and neutralinos are constrained by direct LEP searches and Z pole measurements [62]. This results in log-likelihood values about ten times worse than the minimum. For example, for $\mu = 20$ GeV and variable M_2 the typical Z width is increased by 30 MeV, a large amount compared to the error of 3 MeV and hence ruled out.

In Figure 5 we show the profile likelihoods in the neutralino and chargino sector M_1 , M_2 , and μ for the Planck measurement. All measurements discussed in Section IV are included. The log-likelihood map favors five regions, three of which directly correspond to the mSUGRA case:

1. the stau co-annihilation strip diagonal in M_1 vs M_2 at relatively small values. Here, the mass of the lightest slepton $\tilde{\tau}_1$ is very close to the LSP mass.

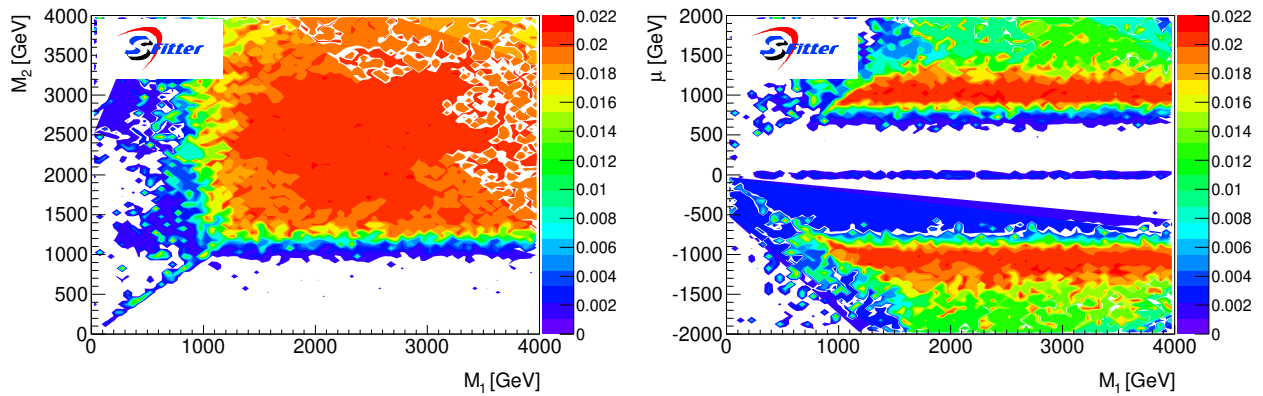


FIG. 5: Profile likelihood projection onto the (M_1, M_2) plane (left) and the (M_1, μ) plane (right) for the Planck measurements.

	co-ann	A-funnel	h-funnel	bino-higgs	higgsino
$\tan \beta$	25	18	26.6	54	29
M_1	430	400	59	800	1543
M_2	788	1500	960	2174	2898
μ	1400	750	484	-800	1070
$M_{\tilde{\mu}_L}$	791	1586	4210	3994	2884
$M_{\tilde{\mu}_R}$	573	2789	4223	1002	2790
$M_{\tilde{\tau}_L}$	747	1067	4062	3744	3355
$M_{\tilde{\tau}_R}$	440	2789	3921	2040	2058
A_τ	-1690	-3038	-2570	2338	-3533
$M_{\tilde{q}_{3L}}$	1744	3938	3162	1683	2210
$M_{\tilde{t}_R}$	1441	3997	2319	2111	2984
A_t	-2142	-3158	-1230	-2162	-3026
m_A	1423	781	3626	1000	784
m_t	174.0	173.5	173.5	173.6	173.5
$-2 \log L/\text{dof}$	47.9/65	44.2/65	46.5/65	42.5/65	37.8/65

	co-ann	A-funnel	h-funnel	bino-higgs	higgsino
$\tilde{\chi}_1^0$	429	398	58.5	768	1066
$\tilde{\chi}_2^0$	783	749	480	-801	-1071
$\tilde{\chi}_3^0$	-1402	-751	-488	829	1545
$\tilde{\chi}_4^0$	1406	1506	969	2178	2900
$\tilde{\chi}_1^\pm$	784	747	480	799	1069
$\tilde{\chi}_2^\pm$	1407	1506	969	2178	2900
h	123.2	125.3	122.1	123.2	124.5
H	1423	781	3626	1000	784
A	1423	781	3626	1000	784
H^\pm	1425	785	3627	1003	788

TABLE IV: Left: examples of best-fit points for the MSSM are shown together with $-2 \log L$ per degrees of freedom. Right: neutralino and chargino masses for the best-fit MSSM points. The masses are given in GeV.

- the A -funnel region where the LSP mass is about half the heavy Higgs mass. This MSSM region behaves the same way as discussed for the simpler mSUGRA model. In Figure 5 it contributes to the bulk region of the M_1 vs M_2 plane as well as to the correlated patterns in the M_1 vs μ plane.
- the h -funnel region at low $M_1 \sim 63$ GeV almost independent of M_2 . Unlike for mSUGRA the gluino mass is now an independent parameter, so the direct LHC searches decouple from the dark matter sector. Because the corresponding MSSM parameter space is tiny, the funnel appears only as distinct sets of points in Figure 5. We have checked that it actually is a narrow line.
- a bino-higgsino region which appears as a strip in the M_1 vs μ plane for $\mu < 0$ and $|M_1| \approx |\mu|$. The dark matter annihilation proceeds through different neutral and charged Higgs-mediated channels, including chargino co-annihilation and dominantly third-generation quarks in the final state. The latter includes the $b\bar{b}$ final state from the A -funnel.
- a large higgsino region with $M_1, M_2 > 1.2$ TeV, split in two almost symmetric solutions $\mu \approx \pm 1.2$ TeV. Because the LSP characteristics in the two regions are very similar we will only refer to $\mu > 0$. Chargino co-annihilation dominates the prediction of the relic density with first and second generation quarks in the final state.

As for the mSUGRA case an additional stop co-annihilation region exists, but is not covered by our parameter range.

In Table IV we give examples for individual best-fitting parameter points in each of these regions. As the parameters are less correlated in the MSSM than in mSUGRA, the top quark mass parameter essentially does not move from its measured value. None of these points are excluded from LHC direct SUSY Higgs searches such as [63]. For the bulk of the solutions the hierarchy in the neutralino sector favors a smaller μ , corresponding to a LSP with a strong higgsino component. Such solutions are hardly realized in strongly constrained models like mSUGRA.

Nevertheless, as every mSUGRA parameter set is contained in the full MSSM, it is important to check that the additional MSSM parameters do not have a large effect on the predictions for the observables and the results of the minimization procedure. For example, the MSSM stau co-annihilation point is similar to the corresponding mSUGRA point: the gaugino mass parameters M_1 and M_2 are the values obtained after the renormalization group evolution from the GUT scale to the electroweak scale, as expected. The MSSM generalization of the A -funnel region shows a similar behavior. The most sensitive measurements are the Higgs boson mass and $\Omega_{\text{cdm}} h^2$, and both are within the theoretical error band. In the h -funnel scenario, $\Omega_{\text{cdm}} h^2$ is very sensitive to the exact value of the Higgs boson mass, the change to the fixed MSSM parameters leads to a change of 150 MeV of the Higgs mass and an increase of $\Omega_{\text{cdm}} h^2$. The bino-higgsino region does not

exist for the mSUGRA model. It is a generalization of the A -funnel, including chargino co-annihilation via a charged Higgs in the s -channel. Essentially mass-degenerate light neutralinos and charginos only appear for light winos or light higgsinos, both not within the range of the renormalization group equations starting from degenerate gaugino masses. For the same reason the higgsino LSP point with chargino co-annihilation through gauge bosons and into light quarks is also absent in the simplified mSUGRA model.

Exploring the MSSM for negative values of M_1 leads to similar structures in the (M_1, M_2) and (M_1, μ) planes. To be precise, while for the (M_1, M_2) plane we observe a mirror symmetry with respect to the M_2 axis, for the (M_1, μ) plane we see a symmetry with respect to a simultaneous change of sign of both M_1 and μ . This observation is corroborated by the study of the parameter sets of Table IV: if only the sign of M_1 is changed, the solution becomes less probable. If additionally the sign of μ is inverted, the mirror solution is as good as the original one. As the neutralino mixing matrix depends on μ and M_1 , a simultaneous change of sign is equivalent to an unobservable global phase for the solutions considered here.

In Figure 6 we show the same parameter constraints as before, but for the WMAP measurement of the relic density. In the (M_1, M_2) plane only a hint of a difference is visible, as WMAP allows for slightly lower M_2 . In the (M_1, μ) plane, WMAP is more compatible in a slightly wider range than Planck with the thin bino–higgsino region identified in Figure 5 (right). On the other hand, WMAP gives slightly looser constraints for larger μ in the higgsino LSP scenario for negative μ . In addition, the h -funnel region is less constrained by the WMAP measurement than by Planck.

As for the mSUGRA analysis, we also compare the profile likelihood with a Bayesian approach. Volume effects can now affect the determination of the model parameters, particularly changing the balance between small and large parameter regions like the h -funnel vs the higgsino regime. As shown in Figure 7, the higgsino LSP region is indeed identified the same way as in the Frequentist projection. The other solutions are more sensitive to volume effects and therefore washed out.

VII. OUTLOOK

Using SFITTER we have studied the impact of measurements coming from cosmological studies ($\Omega_{\text{cdm}} h^2$), direct dark matter searches (Xenon100), and collider measurements (Higgs mass) on the parameter space of the mSUGRA model and on the TeV-scale MSSM. Additional direct and indirect constraints have been included in the analysis, but turned out to be secondary in defining the features of the preferred parameter regions.

We have compared the impact of the measurements of the dark matter relic density by Planck and by WMAP, indicating a very slight shift in the best-fitting parameter points. In contrast, a comparison of profile likelihood and Bayesian methods to reduce the multi-dimensional parameter space showed significant differences, arising

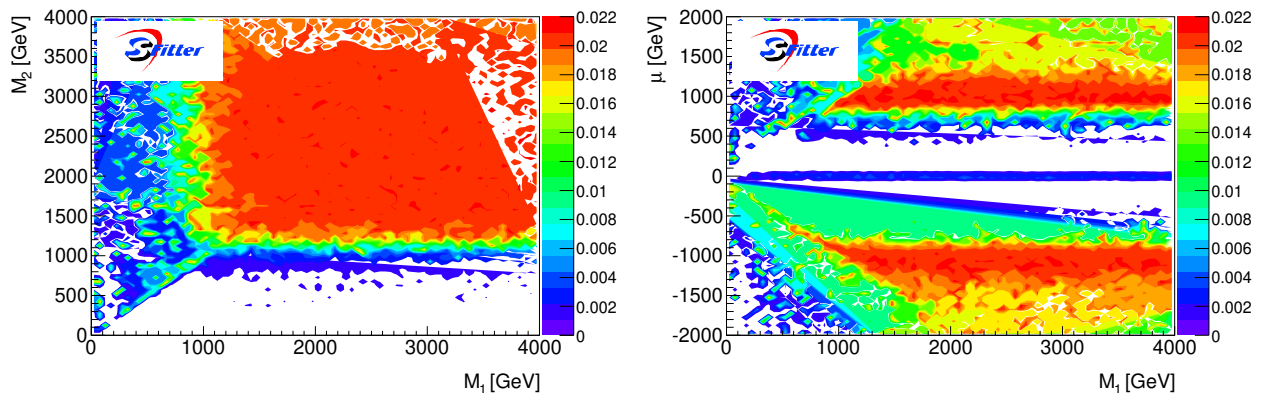


FIG. 6: Profile likelihood projection onto the (M_1, μ) plane (left) and the (M_1, M_2) plane (right) for the WMAP results.

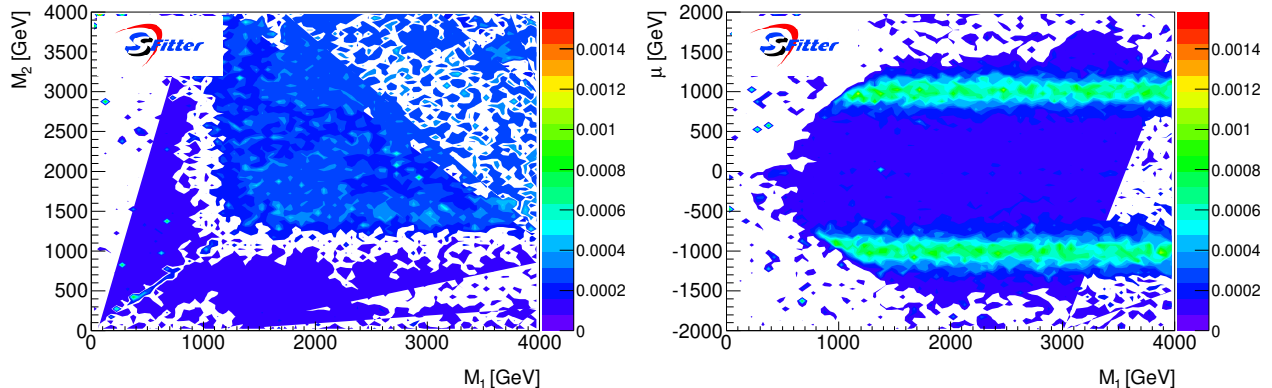


FIG. 7: Bayesian projections onto the (M_1, M_2) plane (left) and the (M_1, μ) plane using the Planck results combined with a $\tan\beta$ -flat prior.

from volume effects and choice of prior. The latter can be chosen either at the GUT scale or at the TeV scale, giving rise to a Jacobian scaling like $\tan^2\beta$.

The allowed regions of supersymmetric parameter space can best be categorized by the dark matter annihilation channel. In mSUGRA we found two valid regions, a narrow stau co-annihilation region at moderate $\tan\beta$ and a large A -funnel region. Stop co-annihilation survives the light Higgs mass constraint, but resides outside our tested range of model parameter space, while the focus-point region seems to be ruled out.

In the TeV-scale MSSM we found narrow allowed regions corresponding to stau co-annihilations and the light-Higgs funnel annihilation. The heavy Higgs funnel becomes part of a large parameter region where the lightest neutralino is a mixed bino-higgsino state, annihilating to third-generation fermions. Chargino co-annihilation occurs with a charged Higgs funnel. In addition, we observed a large higgsino region with chargino and neutralino co-annihilation through gauge boson and into light-flavor quarks. Finally, stop co-annihilation again resides outside our range of model parameters.

Because the allowed regions are very different in size, the Bayesian analysis becomes sensitive to volume effects in comparing dark matter annihilation channels. Moreover, in the light of these categories it is not clear how we would define a simple effective theory covering all these different supersymmetric scenarios, pointing towards a more complex set of effective dark matter models.

In terms of the supersymmetric Lagrangian we found that the positive measurements like the relic density or the Higgs mass generally push supersymmetry toward a high new physics mass scale. The absence of signals for new physics at the 8 TeV run of the LHC puts little tension into the parameter analysis. Nevertheless, several of the parameter regions corresponding to different dark matter annihilation can be probed by the LHC running at 13 TeV. While there is a generic benefit to testing a large variety of dark matter models, the successful simple mSUGRA analysis indicates that there is no immediate need for abandoning the standard WIMP hypothesis for the upcoming LHC run.

Acknowledgments

We would like to thank FITTINO for the stimulating discussions we have had over the past years. We are grateful to Jean-Loic Kneur, Gilbert Moutaka and Michael Ughetto for discussions on the supersymmetric spectrum calculation. We would also like to thank Laurent Duflot for his diligent reading and fruitful comments. TP would like to thank the CCPP at New York University for their hospitality while this paper was finalized. He also wants to thank Neal Weiner for his continuous encouragement to work on an mSUGRA analysis. MR acknowledges partial support by the Deutsche Forschungsgemeinschaft via the Sonderforschungsbereich/Transregio SFB/TR-9 ‘‘Computational Particle Physics’’ and the Initiative and Networking Fund of

the Helmholtz Association, contract HA-101 (“Physics at the Terascale”).

-
- [1] P. W. Higgs, Phys. Lett. **12**, 132 (1964); P. W. Higgs, Phys. Rev. Lett. **13**, 508 (1964); F. Englert and R. Brout, Phys. Rev. Lett. **13**, 321 (1964); ATLAS Collaboration, Phys. Lett. B **716**, 1 (2012); CMS Collaboration, Phys. Lett. B **716**, 30 (2012).
 - [2] E. Aprile *et al.* [XENON100 Collaboration], Phys. Rev. Lett. **107**, 131302 (2011); E. Aprile *et al.* [XENON100 Collaboration], Phys. Rev. Lett. **109**, 181301 (2012)
 - [3] available from: www.sciops.esa.int/index.php?project=planck&page=Planck_Legacy_Archive
 - [4] P. A. R. Ade *et al.* [Planck Collaboration], arXiv:1303.5076 [astro-ph.CO].
 - [5] S. Dawson and H. Georgi, Phys. Rev. Lett. **43**, 821 (1979); M. B. Einhorn and D. R. T. Jones, Nucl. Phys. B **196**, 475 (1982); U. Amaldi, W. de Boer and H. Furstenau, Phys. Lett. B **260**, 447 (1991).
 - [6] for reviews of the MSSM see *e.g.* S. P. Martin, In *Kane, G.L. (ed.): Perspectives on supersymmetry II* 1-153 [hep-ph/9709356]. I. J. R. Aitchison, arXiv:hep-ph/0505105.
 - [7] for early studies see *e.g.* M. S. Carena, J. R. Espinosa, M. Quiros and C. E. M. Wagner, Phys. Lett. B **355**, 209 (1995); H. E. Haber, R. Hempfling and A. H. Hoang, Z. Phys. C **75**, 539 (1997); S. Heinemeyer, W. Hollik and G. Weiglein, Eur. Phys. J. C **9**, 343 (1999); G. Degrassi, S. Heinemeyer, W. Hollik, P. Slavich and G. Weiglein, Eur. Phys. J. C **28**, 133 (2003).
 - [8] H. Goldberg, Phys. Rev. Lett. **50**, 1419 (1983); M. Drees and M. M. Nojiri, Phys. Rev. D **47**, 376 (1993); J. R. Ellis, J. S. Hagelin, D. V. Nanopoulos, K. A. Olive and M. Srednicki, Nucl. Phys. B **238**, 453 (1984); G. Jungman, M. Kamionkowski and K. Griest, Phys. Rept. **267**, 195 (1996); G. Bertone, D. Hooper and J. Silk, Phys. Rept. **405**, 279 (2005).
 - [9] E. Masso, F. Rota and G. Zsembinszki, Phys. Rev. D **70**, 115009 (2004); A. E. Nelson and J. Scholtz, Phys. Rev. D **84**, 103501 (2011); P. Arias, D. Cadamuro, M. Goodsell, J. Jäkel, J. Redondo and A. Ringwald, JCAP **1206**, 013 (2012).
 - [10] L. J. Hall and L. Randall, Nucl. Phys. B **352**, 289 (1991); P. J. Fox, A. E. Nelson and N. Weiner, JHEP **0208**, 035 (2002); Z. Chacko, P. J. Fox and H. Murayama, Nucl. Phys. B **706**, 53 (2005); G. D. Kribs, E. Poppitz and N. Weiner, Phys. Rev. D **78**, 055010 (2008).
 - [11] B. A. Dobrescu, K. Kong and R. Mahbubani, Phys. Lett. B **670**, 119 (2008); M. Gerbush, T. J. Khoo, D. J. Phalen, A. Pierce and D. Tucker-Smith, Phys. Rev. D **77**, 095003 (2008); T. Plehn and T. M. P. Tait, J. Phys. G **36**, 075001 (2009); S. Y. Choi, M. Drees, J. Kalinowski, J. M. Kim, E. Poppenda and P. M. Zerwas, Phys. Lett. B **672**, 246 (2009); ATLAS Collaboration, Eur. Phys. J. C **73**, 2263 (2013). [arXiv:1210.4826 [hep-ex]].
 - [12] see *e.g.* J. Goodman, M. Ibe, A. Rajaraman, W. Shepherd, T. M. P. Tait and H. -B. Yu, Phys. Rev. D **82**, 116010 (2010); P. J. Fox, R. Harnik, J. Kopp and Y. Tsai, Phys. Rev. D **85**, 056011 (2012); S. Profumo, W. Shepherd and T. Tait, arXiv:1307.6277 [hep-ph]; S. Chang, R. Edezhath, J. Hutchinson and M. Luty, arXiv:1307.8120 [hep-ph]; H. An, L. -T. Wang and H. Zhang, arXiv:1308.0592 [hep-ph]; Y. Bai and J. Berger, arXiv:1308.0612 [hep-ph]; A. DiFranzo, K. I. Nagao, A. Rajaraman and T. M. P. Tait, arXiv:1308.2679 [hep-ph]; J. R. Andersen, M. Rauch and M. Spannowsky, arXiv:1308.4588 [hep-ph]; O. Buchmüller, M. J. Dolan and C. McCabe, arXiv:1308.6799 [hep-ph].
 - [13] R. Lafaye, T. Plehn and D. Zerwas, arXiv:hep-ph/0404282; R. Lafaye, T. Plehn, M. Rauch and D. Zerwas, Eur. Phys. J. C **54**, 617 (2008).
 - [14] C. Adam, J. -L. Kneur, R. Lafaye, T. Plehn, M. Rauch and D. Zerwas, Eur. Phys. J. C **71**, 1520 (2011); E. Turlay, R. Lafaye, T. Plehn, M. Rauch and D. Zerwas, J. Phys. G **38**, 035003 (2011).
 - [15] R. Lafaye, T. Plehn, M. Rauch, D. Zerwas and M. Dührssen, JHEP **0908**, 009 (2009); M. Klute, R. Lafaye, T. Plehn, M. Rauch and D. Zerwas, Phys. Rev. Lett. **109**, 101801 (2012); D. Lopez-Val, T. Plehn and M. Rauch, arXiv:1308.1979 [hep-ph].
 - [16] G. Hinshaw *et al.* [WMAP Collaboration], arXiv:1212.5226 [astro-ph.CO].
 - [17] L. E. Ibañez, Phys. Lett. B **118**, 73 (1982); J. R. Ellis, D. V. Nanopoulos and K. Tamvakis, Phys. Lett. B **121**, 123 (1983); L. Alvarez-Gaumé, J. Polchinski and M. B. Wise, Nucl. Phys. B **221**, 495 (1983); K. Inoue, A. Kakuto, H. Komatsu and S. Takeshita, Prog. Theor. Phys. **68**, 927 (1982) [Erratum-ibid. **70**, 330 (1983)]; A. H. Chamseddine, R. Arnowitt and P. Nath, Phys. Rev. Lett. **49**, 970 (1982).
 - [18] P. Bechtle, K. Desch and P. Wienemann, arXiv:hep-ph/0412012; P. Bechtle, T. Bringmann, K. Desch, H. Dreiner, M. Hamer, C. Hensel, M. Krämer and N. Nguyen *et al.*, JHEP **1206** (2012) 098.
 - [19] O. Buchmüller, R. Cavanaugh, M. Citron, A. De Roeck, M. J. Dolan, J. R. Ellis, H. Flacher and S. Heinemeyer *et al.*, Eur. Phys. J. C **72**, 2243 (2012)
 - [20] C. Boehm, P. S. B. Dev, A. Mazumdar and E. Pukartas, JHEP **1306**, 113 (2013).
 - [21] T. Cohen and J. G. Wacker, arXiv:1305.2914 [hep-ph].
 - [22] A. Fowlie, M. Kazana, K. Kowalska, S. Munir, L. Roszkowski, E. M. Sessolo, S. Trojanowski and Y. -L. S. Tsai, Phys. Rev. D **86**, 075010 (2012); A. Fowlie, K. Kowalska, L. Roszkowski, E. M. Sessolo and Y. -L. S. Tsai, Phys. Rev. D **88**, 055012 (2013);

- [23] see *e.g.* L. Roszkowski, E. M. Sessolo and Y. -L. S. Tsai, Phys. Rev. D **86**, 095005 (2012); C. Strege, G. Bertone, F. Feroz, M. Fornasa, R. Ruiz de Austri and R. Trotta, JCAP **1304**, 013 (2013); B. Bhattacharjee, M. Chakraborti, A. Chakraborty, U. Chattopadhyay, D. Das and D. K. Ghosh, arXiv:1305.4020 [hep-ph]; M. Cahill-Rowley, J. Hewett, A. Ismail and T. Rizzo, arXiv:1308.0297 [hep-ph]; please send us email if you have an excellent reason to be on this list.
- [24] A. Djouadi, J. -L. Kneur and G. Moultaka, Comput. Phys. Commun. **176**, 426 (2007).
- [25] M. Drees and S. P. Martin, arXiv:hep-ph/9504324. Note that in this reference the off-diagonal entry of the stop mass matrix is given by $m_t(A_t + \mu \cot \beta)$, *i.e.* their sign convention for the A parameters is opposite to ours.
- [26] J. A. Aguilar-Saavedra, A. Ali, B. C. Allanach, R. L. Arnowitt, H. A. Baer, J. A. Bagger, C. Balazs and V. D. Barger *et al.*, Eur. Phys. J. C **46**, 43 (2006). [hep-ph/0511344].
- [27] B. C. Allanach, K. Cranmer, C. G. Lester and A. M. Weber, JHEP **0708**, 023 (2007).
- [28] B. C. Allanach, Comput. Phys. Commun. **143**, 305 (2002).
- [29] for a detailed discussion of these correlations see J. Jaeckel, V. V. Khoze, T. Plehn and P. Richardson, Phys. Rev. D **85**, 015015 (2012).
- [30] A. Djouadi, J. Kalinowski and M. Spira, Comput. Phys. Commun. **108**, 56 (1998); M. Mühlleitner, A. Djouadi and Y. Mambrini, arXiv:hep-ph/0311167; A. Djouadi, M. M. Mühlleitner and M. Spira, Acta Phys. Polon. B **38**, 635 (2007).
- [31] G. Belanger, F. Boudjema, P. Brun, A. Pukhov, S. Rosier-Lees, P. Salati and A. Semenov, Comput. Phys. Commun. **182**, 842 (2011).
- [32] S. Heinemeyer, W. Hollik, A. M. Weber and G. Weiglein, JHEP **0804**, 039 (2008). A. Weber, private communication.
- [33] K. Griest and D. Seckel, Phys. Rev. D **43**, 3191 (1991); S. Mizuta and M. Yamaguchi, Phys. Lett. B **298**, 120 (1993); J. R. Ellis, T. Falk and K. A. Olive, Phys. Lett. B **444**, 367 (1998); J. R. Ellis, T. Falk, K. A. Olive and M. Srednicki, Astropart. Phys. **13**, 181 (2000) [Erratum-ibid. **15**, 413 (2001)].
- [34] J. R. Ellis, K. A. Olive and Y. Santoso, Astropart. Phys. **18**, 395 (2003).
- [35] P. Binetruy, G. Girardi and P. Salati, Nucl. Phys. B **237**, 285 (1984); S. Mizuta and M. Yamaguchi, Phys. Lett. B **298**, 120 (1993); J. Edsjo and P. Gondolo, Phys. Rev. D **56**, 1879 (1997).
- [36] J. L. Feng, K. T. Matchev and F. Wilczek, Phys. Lett. B **482**, 388 (2000).
- [37] ATLAS Collaboration, Phys. Rev. D **87**, 012008 (2013).
- [38] CMS Collaboration, CMS-PAS-SUS-12-005.
- [39] ATLAS Collaboration, Science **338**, 1576 (2012).
- [40] R. Aaij *et al.* [LHCb Collaboration], Phys. Rev. Lett. **110**, 021801 (2013).
- [41] CMS Collaboration, Phys. Rev. Lett. **111**, 101804 (2013).
- [42] Particle Data Group <http://pdg.lbl.gov/2012/reviews/rpp2012-rev-b-meson-prod-decay.pdf>
- [43] Particle Data Group <http://pdg.lbl.gov/2012/reviews/rpp2012-rev-g-2-muon-anom-mag-moment.pdf>
- [44] Particle Data Group: <http://pdg.lbl.gov/2012/reviews/rpp2012-rev-standard-model.pdf>
- [45] ATLAS Collaboration, Phys. Lett. B **710** 383 (2012); ATLAS Collaboration, Phys. Rev. Lett. **108** 111803 (2012); ATLAS Collaboration, Phys. Lett. B **716** 62 (2012); ATLAS Collaboration, JHEP **1209** 070 (2012); ATLAS Collaboration, Phys. Rev. D **86** 032003 (2012); ATLAS Collaboration, Phys. Lett. B **716** 1 (2012); CMS Collaboration, Phys. Lett. B **710** 91 (2012); CMS Collaboration, Phys. Rev. Lett. **108** 111804 (2012); CMS Collaboration, Phys. Lett. B **710** 284 (2012); CMS Collaboration, Phys. Lett. B **713** 68 (2012).
- [46] see *e.g.* P. Bechtle, S. Heinemeyer, O. Stal, T. Stefaniak, G. Weiglein and L. Zeune, Eur. Phys. J. C **73**, 2354 (2013); G. D. Kribs, A. Martin and A. Menon, arXiv:1305.1313 [hep-ph]; A. Djouadi, L. Maiani, G. Moreau, A. Polosa, J. Quevillon and V. Riquer, arXiv:1307.5205 [hep-ph].
- [47] R. Aaij *et al.* [LHCb Collaboration], Phys. Rev. Lett. **111**, 101805 (2013).
- [48] C. L. Bennett *et al.* [WMAP Collaboration], arXiv:1212.5225 [astro-ph.CO].
- [49] C. L. Reichardt, R. de Putter, O. Zahn and Z. Hou, Astrophys. J. **749**, L9 (2012); S. Das, T. Louis, M. R. Nolte, G. E. Addison, E. S. Battistelli, J. R. Bond, E. Calabrese and D. C. M. J. Devlin *et al.*, arXiv:1301.1037 [astro-ph.CO].
- [50] F. Beutler, C. Blake, M. Colless, D. H. Jones, L. Staveley-Smith, L. Campbell, Q. Parker and W. Saunders *et al.*, Mon. Not. Roy. Astron. Soc. **416**, 3017 (2011); N. Padmanabhan, X. Xu, D. J. Eisenstein, R. Scalzo, A. J. Cuesta, K. T. Mehta and E. Kazin, Mon. Not. Roy. Astron. Soc. **427**, no. 3, 2132 (2012); L. Anderson, E. Aubourg, S. Bailey, D. Bizyaev, M. Blanton, A. S. Bolton, J. Brinkmann and J. R. Brownstein *et al.*, Mon. Not. Roy. Astron. Soc. **427**, no. 4, 3435 (2013).
- [51] A. G. Riess, L. Macri, S. Casertano, H. Lampeitl, H. C. Ferguson, A. V. Filippenko, S. W. Jha and W. Li *et al.*, Astrophys. J. **730**, 119 (2011) [Erratum-ibid. **732**, 129 (2011)].
- [52] for a recent update see *e.g.* A. Arbey, M. Battaglia, F. Mahmoudi and D. Martinez Santos, Phys. Rev. D **87**, 035026 (2013).
- [53] see *e.g.* H. Baer and M. Brhlik, Phys. Rev. D **55**, 3201 (1997).
- [54] for a review on new-physics effects see *e.g.* D. Stöckinger, J. Phys. G **34**, R45 (2007).
- [55] A. Höcker, H. Lacker, S. Laplace and F. Le Diberder, Eur. Phys. J. C **21**, 225 (2001).
- [56] A. Gelman and D. B. Rubin, Statist. Sci. **7** 457 (1992).

- [57] B. C. Allanach and C. G. Lester, Phys. Rev. D **73** 015013 (2006).
- [58] F. James and M. Roos, Comput. Phys. Commun. **10**, 343 (1975).
- [59] A. M. Ferrenberg, R. H. Swendsen, Phys. Rev. Lett. **61**, 2635 (1988).
- [60] B. C. Allanach *et al* , Eur. Phys. J. C **25**, 113 (2002).
- [61] see *e.g.* T. Plehn, D. Rainwater and P. Skands, Phys. Lett. B **645**, 217 (2007); H. K. Dreiner, M. Krämer and J. Tattersall, Europhys. Lett. **99**, 61001 (2012).
- [62] S. Schael *et al.* [ALEPH and DELPHI and L3 and OPAL and SLD and LEP Electroweak Working Group and SLD Electroweak Group and SLD Heavy Flavour Group Collaborations], Phys. Rept. **427** 257 (2006).
- [63] ATLAS Collaboration, JHEP **1302** 095 (2013); [arXiv:1211.6956 [hep-ex]],
CMS Collaboration, Phys. Lett. B **722** 207 (2013) [arXiv:1302.2892 [hep-ex]].